Nonlinear Site Response at a Soft Port Site

Vertical-Array Constraints for California's Liquefaction-Susceptible Waterfronts

Ken Hudson[1] [1]Hudson Geotechnics, Inc. · ken@hudsongeotechnics.com

SCEC 2026 Annual Meeting
Palm Springs, CA

1. Why this site

Nonlinear site response is among the least constrained contributors to ground-motion uncertainty in California, and it matters most where records are scarcest — the soft, saturated hydraulic fills beneath the Ports of Los Angeles and Long Beach. Vertical arrays that capture strong shaking on such profiles are rare.

The PARI array at Yatsushiro Port, Kumamoto, pairs a surface accelerometer with a downhole sensor at 34.43 m in a V_{S30} = 169 m/s profile: water table at 2–3 m, SPT N below 10 through most of the upper 30 m, and a velocity inversion at 24–29 m where N falls to 1–3.

On 28 July 2026 an **M**6.8 earthquake ruptured the Futagawa–Hinagu fault system. The Yatsushiro Port array sits on the rupture's surface projection (R_{jb} ≈ 0–2 km, R_{rup} ≈ 5 km). Liquefaction induced settlement and sand ejecta was observed and measured at the downhole array location after the event.

An observation of liquefaction manifestation, measured free-field settlement, and a downhole/surface record pair makes this a very unique and valuable dataset.

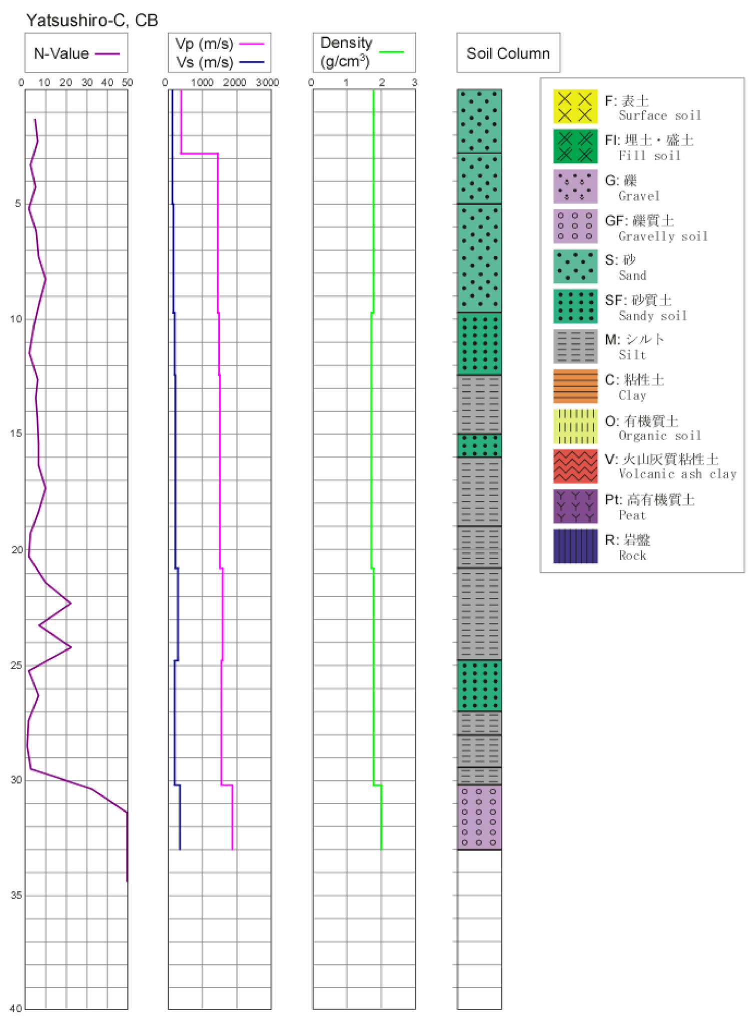

Figure 1: Yatsushiro Port downhole array soil profile properties.

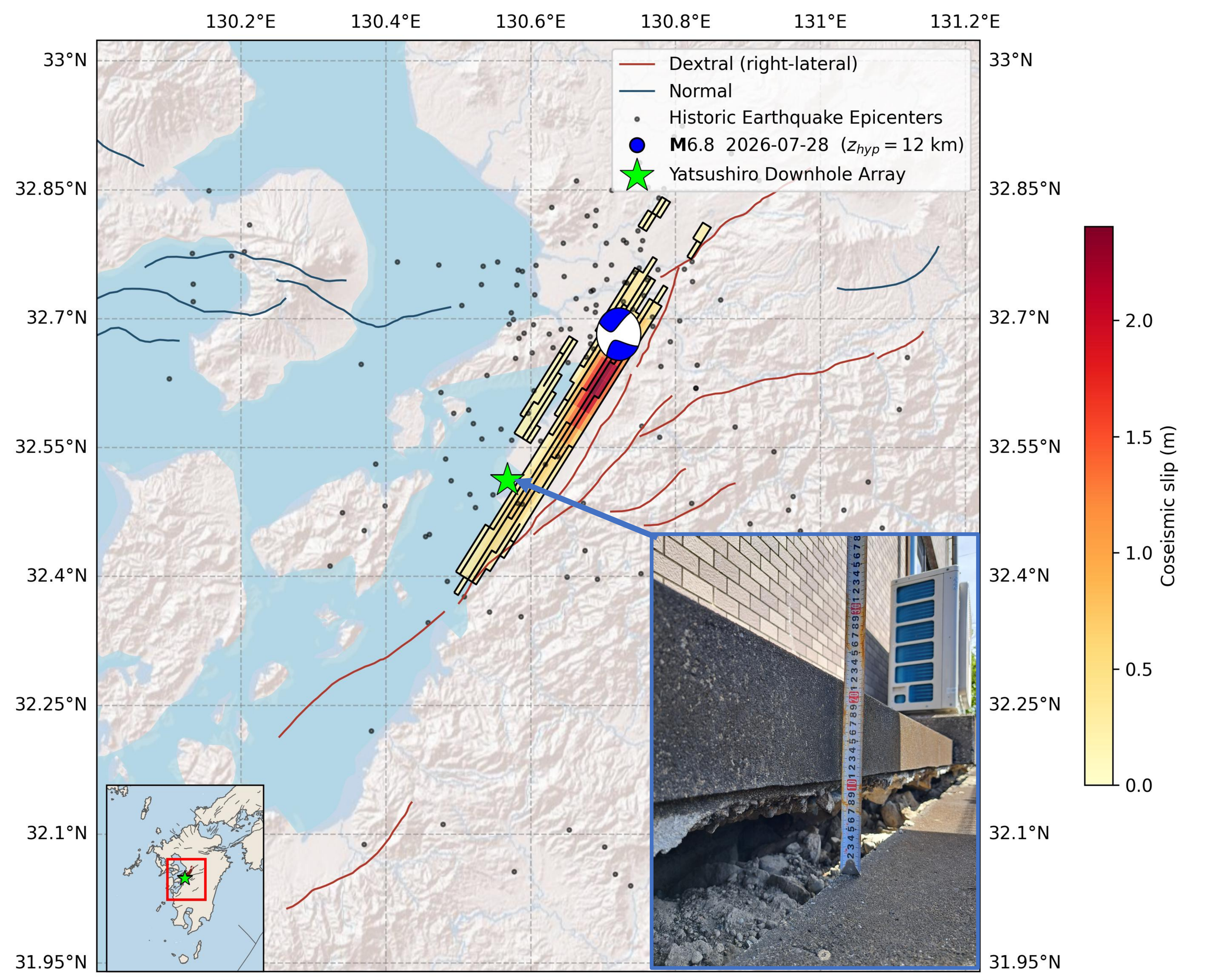

Figure 2: Rupture context. Finite-fault coseismic slip (color), the moment tensor, GEM active faults and M ≥ 3 historic epicenters. The Yatsushiro downhole array (star) lies on the surface projection of the rupture, ~5 km from the fault plane. Inset photo was taken at the location of the seismometer showing settlement of the ground surface relative to a pile supported building that is adjacent to the downhole array.

2. Nonlinear (liquefied) site response

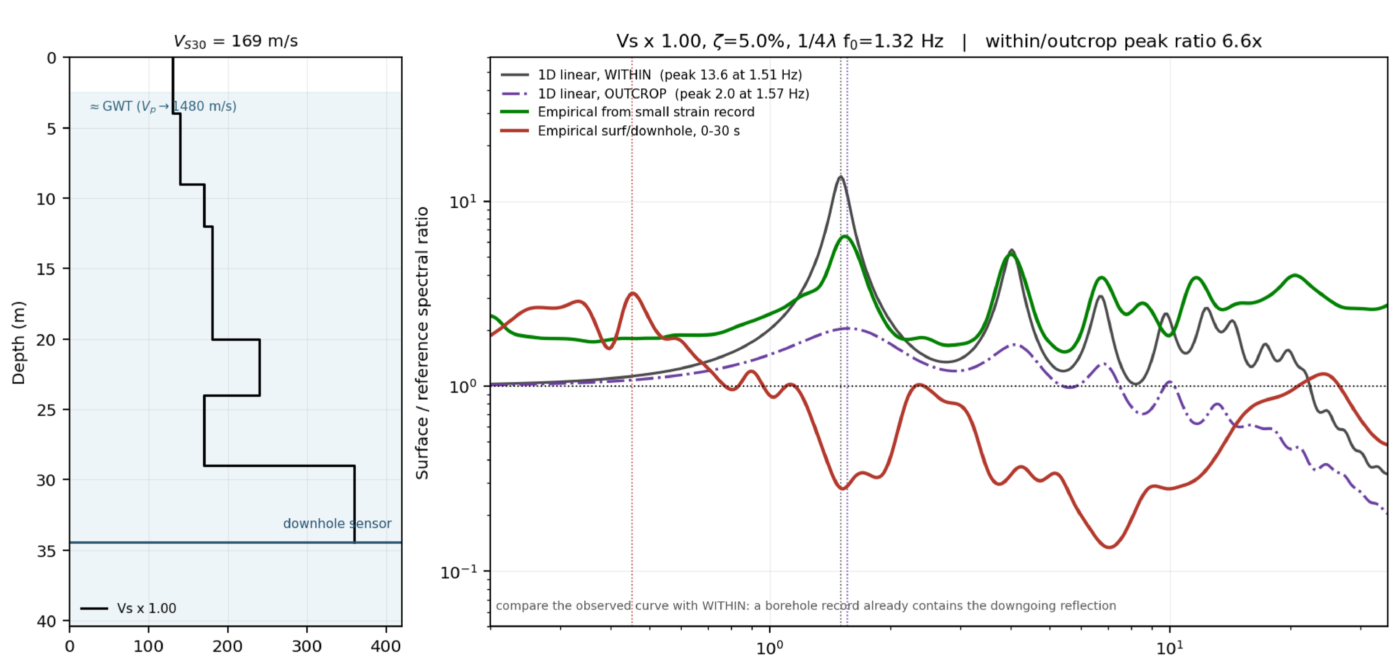

Figure 3: V_s profile and transfer functions. 1D linear theory predicts resonance at 1.51 Hz amplifying 13.6× (within-motion). The mainshock (red) peaks at 0.45 Hz amplifying 3× and falls below unity from 1.5 to 15 Hz — the column low-pass filtered the motion instead of amplifying it.

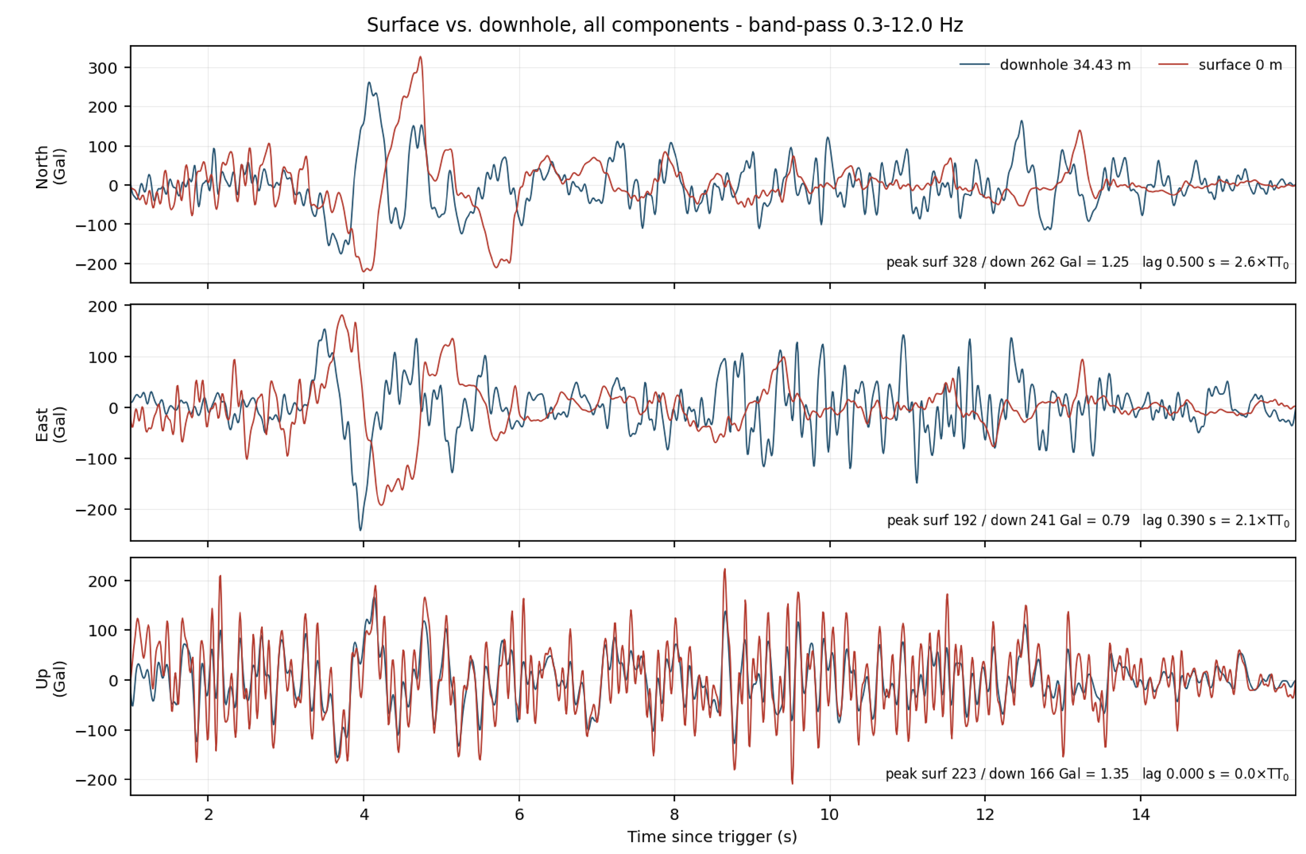

Figure 4: Surface and downhole overlaid, 0.3–12 Hz. The surface trace is smoother, lower in frequency and visibly delayed: one-way travel time reaches 0.50 s on North, 2.6× the small-strain value. PGA is barely amplified — 1.25 (N) and 0.79 (E).

3. When does it soften?

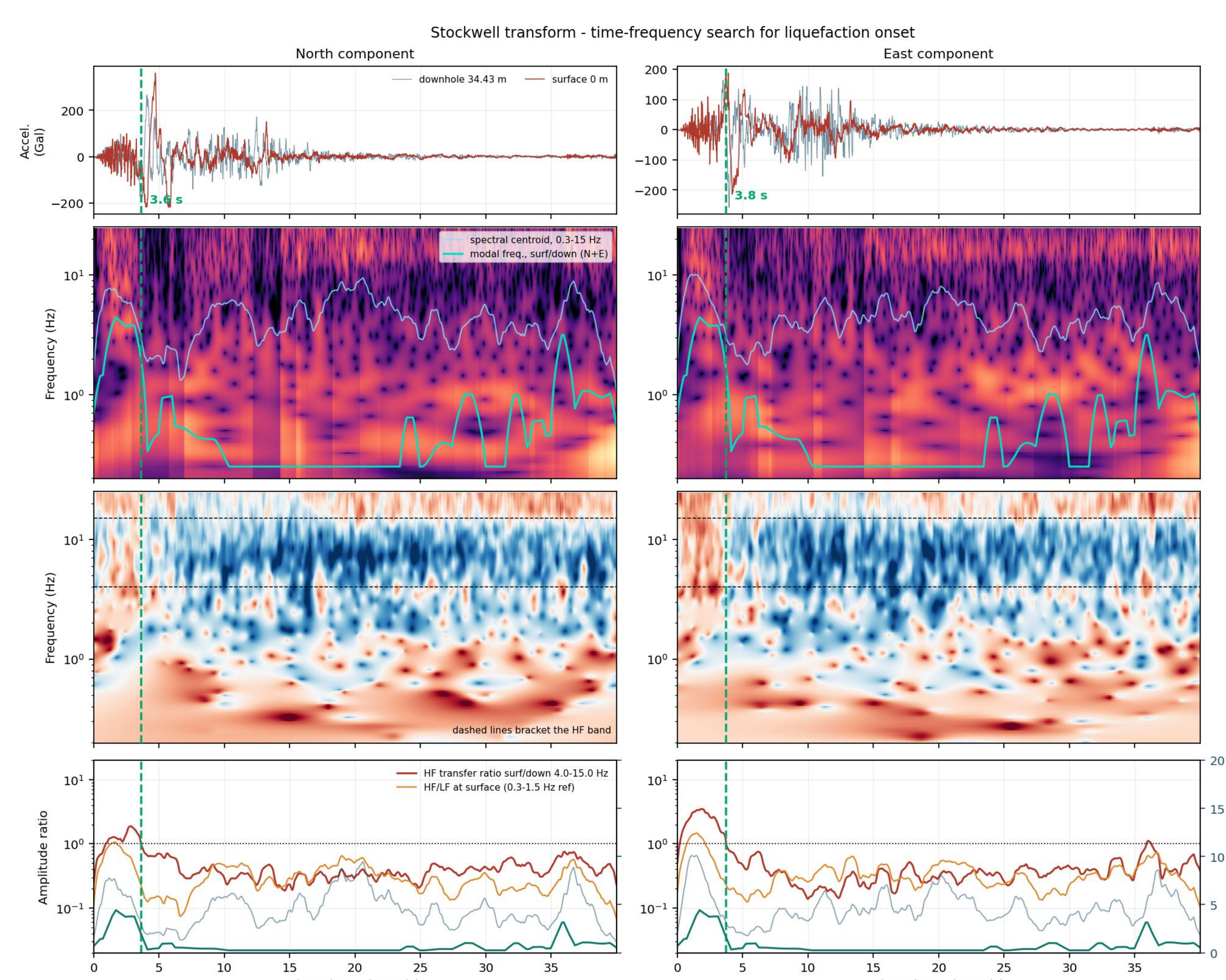

Figure 5: Stockwell transform of the mainshock, normalized per time step. Panel rows: waveforms; $|S|^2$ at the surface with modal frequency; surface/downhole ratio; band ratios. Transmission through 4–15 Hz collapses at 3.6 s (N) and 3.8 s (E) — about one second before peak acceleration. Taking the ratio between sensors removes the input motion, so the change is the soil's, not the earthquake's.

3.6 s
onset of high-frequency decoupling, from four independent estimators

0.45 Hz
mainshock f_0 (weak-motion reference 1.73 Hz)

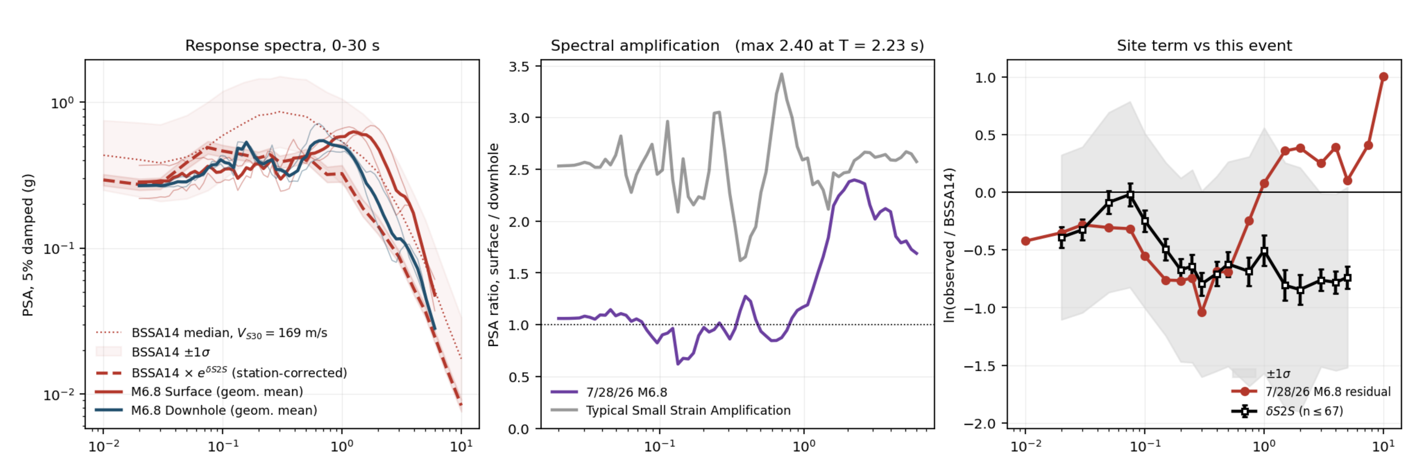

Figure 6: 5%-damped response spectra. Deamplification through 0.1–0.8 s and 2.4× amplification near 2.2 s.

Methods. Konno-Ohmachi spectral ratios (b = 30); bounded cross-correlation with parabolic sub-sample peak interpolation; Stockwell transform normalised per time step; deconvolution interferometry with multitaper spectra. Every estimate is quality-controlled against band-edge pinning, cycle skips and pre-trigger mis-detection — 21 of 213 events excluded. Sampling rate (100 Hz) is inferred from the inter-sensor travel time, the anti-alias corner and κ, not read from a header.

4. Calibrating against 213 events

A single record cannot say what "linear" means at a site. I processed the full PARI catalogue at this array — 213 surface/downhole pairs, M 1.1–7.1 — to measure the reference rather than borrow it from the V_s log.

Weak-motion records that follow a large event are still softened. Excluding those inside a 14-day healing window changes the answer: the clean reference travel time is 199 ms, only 5% off the borehole log, where the contaminated one was 16% off.

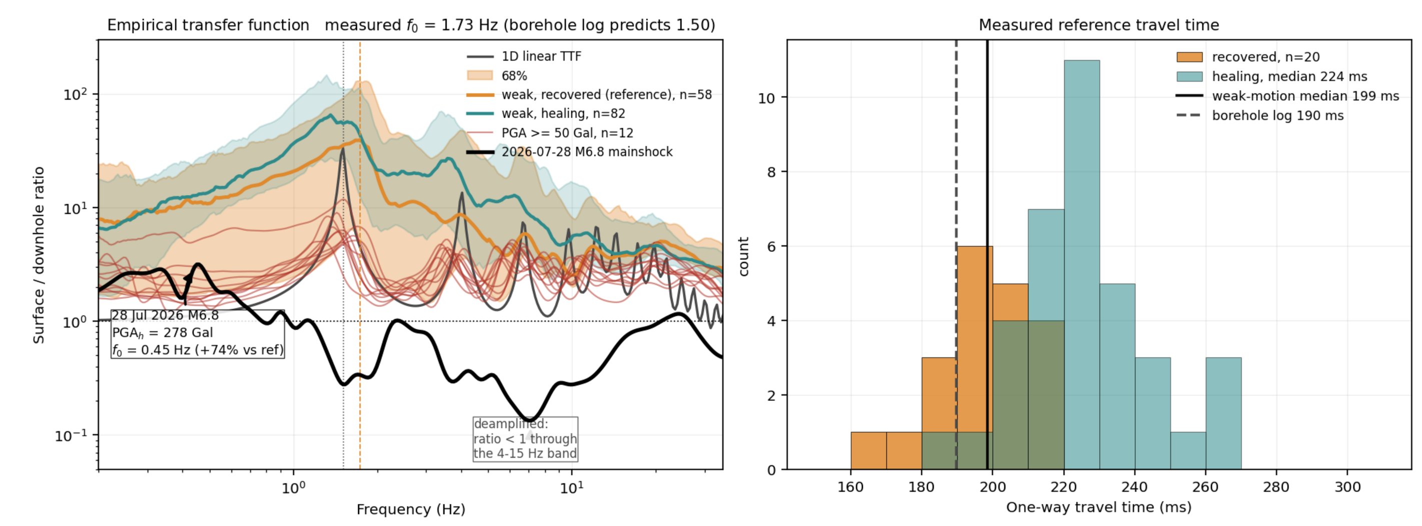

Figure 7: Measured reference. Left: weak-motion transfer function (orange) versus records still inside a healing period (teal); f_0 = 1.73 Hz against 1.51 Hz predicted. Right: travel-time populations separate cleanly — recovered records cluster at the borehole-log value, healing records 25 ms slower.

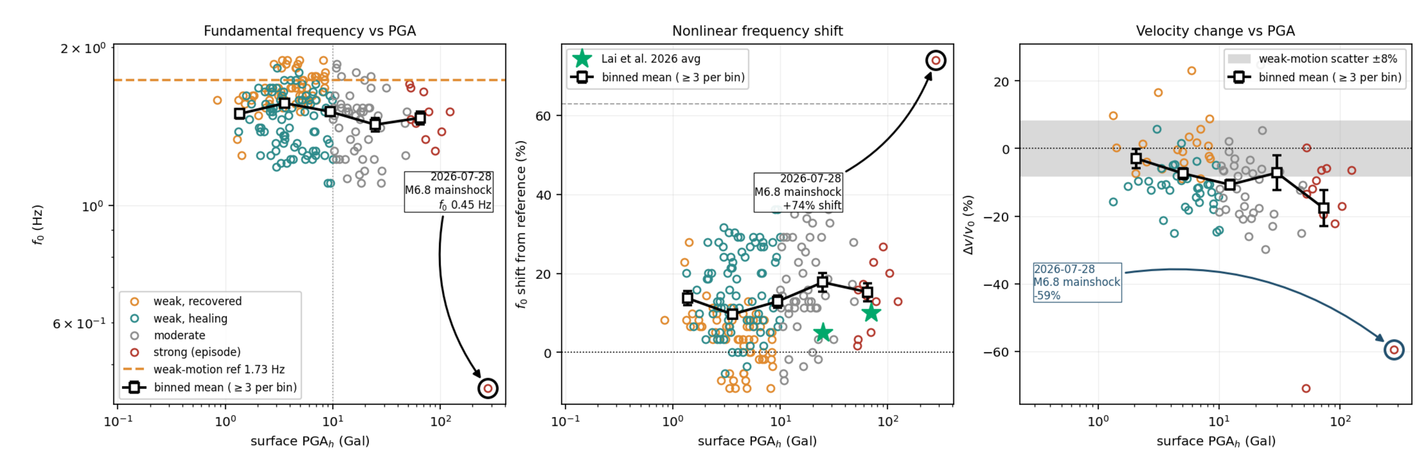

Figure 8: f_0 and $\Delta v/v_0$ against PGA, coloured by category, with binned means. The mainshock shifts f_0 by +74% and velocity by −59%. Weak-motion scatter (grey band, ±8%) is the uncertainty on any single event.

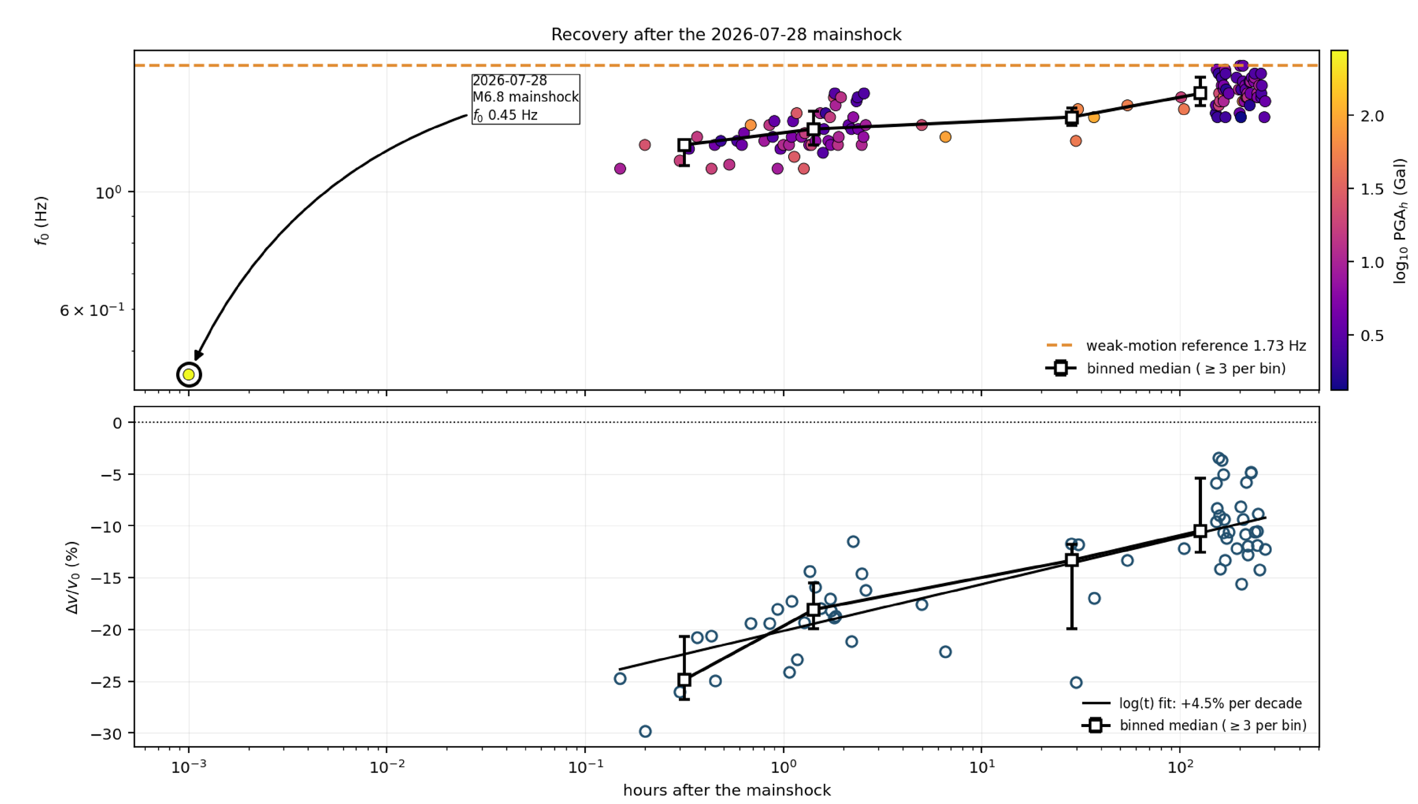

Figure 9: Recovery through the aftershock sequence. $\Delta v/v_0$ improves from −25% at 0.3 h to −10% at 200 h, following log(t) at +4.5% per decade — and does not close. Referenced against uncontaminated weak motion, healing is incomplete after 11 days.

5. Takeaways

- A Site Class E profile produced essentially no PGA amplification. Linear 1D theory over-predicted the resonant amplification by ~4× and missed the resonance by more than an octave. Nonlinear GMM predictions overestimate short period attenuation and underestimate the long period amplification caused by liquefaction
- Four independent estimators — spectral ratio, modal frequency, cross-correlation travel time, deconvolved impulse response — agree on 3.6 s onset and a 55–60% velocity loss.
- In-situ μ/μ_0 reached 0.16 at γ ≈ 1%, against 35% velocity loss reported by Efsahani et al. (2024) for the 2016 M 7.2 on this same fault system.
- Weak-motion references must exclude the aftershocks of strong events, or apparent recovery is measured against already-softened ground.

Data: PARI strong-motion network (eq.pari.go.jp). Faults: GEM GAF-DB (Styron & Pagani 2020). Methods after Bonilla, Guéguen & Ben-Zion (2019); Lai et al. (2026); Kristeková et al. (2026).

HUDSON GEOTECHNICS